

Oblique Point-Focusing Shear-Horizontal Guided – Wave Electromagnetic Acoustic Transducer with Variable PPM Spacing

Hongyu Sun, Shen Wang, Songling Huang*, *Senior Member, IEEE*, Lisha Peng, Qing Wang, *Senior Member, IEEE*, and Wei Zhao

Abstract— We realized a phase-coherent oblique point-focusing shear-horizontal (SH) guided-wave electromagnetic acoustic transducer (EMAT) composed of variable-spacing periodic permanent magnets (PPMs) and racetrack coils. For traditional focusing transducers, the necessary focal position adjustment in defect detection requires a redesign of the coil structure. More conveniently, this new transducer structure arrangement can achieve wave focusing and focal position change by rationally adjusting the layout of the periodic permanent magnet without changing the coil structure. Simulation results show that this newly designed transducer has good focusing performance: it can successfully focus the signal to a preset point, and the signal amplitude is nearly double that of the nonfocusing side. In addition, the focusing performance optimization of the transducer has been studied. The experimental results agree well with the actual location and size of a defect, which verifies the effectiveness of the newly designed focusing transducer in defect detection.

Index Terms— Electromagnetic acoustic transducer (EMAT), oblique point-focusing shear-horizontal (SH) guided wave, variable periodic permanent magnet (PPM) spacing.

I. INTRODUCTION

The quality control of a product can reflect the industrial level of the country to a certain extent. Nondestructive testing (NDT), as a technology that is both economical and capable of meeting product performance requirements, can be used as a method to evaluate the internal structure and physical properties of products without damaging equipment or materials [1-5]. Testing methods that are widely used in industry include magnetic flux leakage, radiation, magnetic particles, eddy currents, and ultrasonication. Ultrasonic wave detection, as one of the NDT technologies, is rapid, can be used for long-distance detection and has good environmental

adaptability, and is currently widely used in industry. It is a method used to determine whether a specimen has defects by using the propagation characteristics of the ultrasonic wave, namely, reflection, transmission, and refraction [6-10].

Currently, the piezoelectric ultrasonic transducer based on the piezoelectric principle is most widely used in NDT [11]. It transmits the excited electrical pulses to the piezoelectric chip, thereby generating mechanical vibrations of the same frequency, which excites the ultrasonic waves. Although this transducer is widely used because it has a high energy conversion efficiency, is easy to operate, and is a mature technology, it also has limits, such as the couplant required, the harsh environment, and the difficulty of exciting specific wave modes. Therefore, noncontact ultrasonic techniques, including laser ultrasonication and electromagnetic acoustic transducers (EMATs), are becoming more widely accepted [12]. The EMAT consists of a permanent magnet that provides a background magnetic field, a coil that provides eddy currents, and a specimen that transmits ultrasonic waves. Its main advantages include that there is no need for a couplant and its adaptability to harsh environments, and mode control [13-15]. However, a common problem with these transducers is the low energy conversion efficiency, which causes problems for defect detection purposes. Therefore, improving the energy conversion efficiency of an EMAT is vital.

Focusing ultrasound is an effective method for solving this problem. Because this method does not have high requirements for additional complex amplifier circuits, only a reasonable design and optimization of the transducer structure are required to achieve high-precision and high-efficiency defect detection. Many scholars have studied guided-wave and surface-wave focusing EMATs and successfully applied them for the defect detection of metal plates and pipelines [16-19]. For the detection using body waves, a shear vertical (SV) wave is widely used as an ultrasonic wave that propagates obliquely inside the test specimen in the field of rail, tank floor, and oil pipeline detection. The focusing method of the SV wave was first proposed by Ogi [20]. In his study, a sharp focusing of SV wave beams was achieved by regarding the neighboring two spacings as a unit source, and the EMAT showed a pronounced sensitivity for flaw detection. However, constructive interference cannot be guaranteed using this method due to the asymptotic nature of the hyperbola. Therefore, Ogi redesigned

*Correspondence to: Songling Huang. (Email: huangsling@tsinghua.edu.cn) State Key of Power Systems, Department of Electrical Engineering, Tsinghua University, Beijing, 10084, China
Hongyu Sun, Shen Wang, Songling Huang, Lisha Peng, and Wei Zhao are with the State Key Lab. of Power System, Department of Electrical Engineering, Tsinghua University, Beijing 100084, China.
Q. Wang is with the Department of Engineering, Durham University, Durham DH1 3LE, U.K.

the coil structure according to the Huygens principle to achieve phase focusing of the SV wave at the focal line position [21]. In his research, sharp amplitude peaks appear in both the direction and position of the designed focal line, both in generation and reception. For SH wave focusing, Alers et al. have proposed methods based on phase coherence at a focal point and developed both SH and SV wave focusing EMATs [22]. SH wave focusing method based on magnetostrictive mechanism is applied to weld inspection for a steel. However, he did not give the detailed structure and specific application of SH-EMAT. For guided wave focusing, although the problems of shear horizontal (SH) guided wave focusing regarding the fabrication accuracy, process level, and optimization of transducer parameters were mentioned in his research twenty years ago, these disadvantages can be solved today. Hill found that the beam directivity of the SH guided wave EMAT using the periodic permanent magnet (PPM) can be controlled by changing the drive frequency [23, 24]. However, he did not further study the advantages of the directional focusing of SH guided waves. Moreover, further achievement of the phase focusing of guided-waves compared to beam focusing is more effective and important for improving the energy conversion efficiency of an EMAT. Compared with our latest research results [25], the structure of the focusing transducer has been greatly simplified in this paper, and the new EMAT is suitable for oblique focusing requirements.

In this work, we developed a beam-focusing SH guided-wave EMAT and proposed a point-focusing phase-coherent EMAT that can effectively improve the energy conversion efficiency of the transducer with satisfactory defect detection accuracy. First, we analyze the effect of two parameters on the wave propagation direction, namely, the excitation frequency and the source spacing, and develop an EMAT that can achieve directional beam focusing. Next, we propose a newly designed SH guided-wave EMAT that can achieve phase-coherent point focusing and improve the energy conversion efficiency of the transducer. Through wavefield calculation based on the Huygens approximation, the relationship between the wavefield intensity at different positions over time is obtained. Then, to obtain a more accurate wavefield distribution, a finite element method is used to simulate the newly designed point focusing EMAT, and the relevant parameters at the focal position are obtained. Then, the effects of the unit source size and number are investigated. Finally, an experiment is implemented to detect defects on the specimen, which proves the effectiveness of the newly designed focusing EMAT.

II. THEORETICAL ANALYSIS

There are two main purposes for focusing ultrasonic guided waves: improving the beam directivity and enhancing the sound field intensity. The corresponding implementation methods are to change the spacing of the radiation sources, but their principles are different: one is to implement beam steering but ignores an equal phase, and the other is to ensure coherency for all beams without considering the beam's directional focusing. The first method solves the problem of the broad radiation pattern of an ultrasound wave, and the second method improves

the low energy conversion efficiency, which is the main drawback of all EMATs. Moreover, the beam steering of SH guided waves was proposed and well-studied by Hill [23, 24], and it is more important to achieve equal-phase focusing, as discussed above [21]. Therefore, we propose the beam-focusing method of an SH guided-wave EMAT and study the characteristics of the new phase-coherent point-focusing SH guided-wave EMAT in detail.

A. Beam steering

The polarization direction of SH guided waves exists only in the plane; no off-plane displacement occurs. Therefore, we can consider simplifying the analysis to a 2D model, as shown in Fig. 1(a). Rectangles with different colors and fills represent radiation sources of opposite polarity (permanent magnets of different polarities) with respect to the y-axis. Here, d represents the distance between two radiation sources of the same polarity, θ is defined as the radiation angle, n is a nonnegative integer, and λ is the wavelength, which is related to the shear wave velocity and drive frequency. The equation in Fig. 1(a) shows that constructive interference can be achieved by using equally spaced radiation sources. This directional control of the source array can be described as follows [23]

$$d(\theta) = \int_0^\infty S(\omega) \sin c \left(\frac{\omega l \sin \theta}{2c_s} \right) \sum_{n=0}^N (-1)^n e^{in\omega d \sin \theta / 2c_s}, \quad (1)$$

where $S(\omega)$ is the input signal and ω is the angular frequency. The size of a radiation source is $w \times l$, as shown in Fig. 1(f). This equation represents the total contribution of all sources to an input signal containing different frequency components. In this way, we can calculate and analyze two factors that affect the beam directivity: the distance d and the frequency f . Figs. 1(b, c) show the relationship between d and radiation angle θ . Here, $l=1.5$ mm, $c_s=3200$ m/s, $N=6$, and $f=1$ MHz. It can be seen that as d increases, θ and the beam width decrease. For Figs. 1(d, e), f is selected as a variable, while d is fixed at 6 mm. θ and the beam width decrease as the input signal frequency f increases. Based on the theory above, we propose a method to focus wave beams radiated by all sources using variable spacing sources as depicted in Fig. 1(f). In the research on directional focusing, the midpoint of two vibration sources is generally selected as the radiation point for elastic waves [20]. Here, x_i denotes the x-coordinate of the i -th vibration source, b_i is the distance between the i -th and $(i+1)$ -th vibration sources, θ_i represents the radiation angle of the i -th radiation source, (x_f, y_f) is the coordinate of the focal point, and r_i is the distance between the i -th radiation source and the focal point. By using the equation in Fig. 1(f), beam steering and focusing can be achieved. Although this method can be used for the beam focusing of SH guided-waves, it does not focus on the most significant problem, i.e., low conversion efficiency, which must urgently be solved for EMATs; thus, this paper will not go into further details.

B. Coil arrangement

A new and alternative way to focus ultrasonic guided-waves is proposed in this paper to achieve phase coherence. Fig. 2(a)

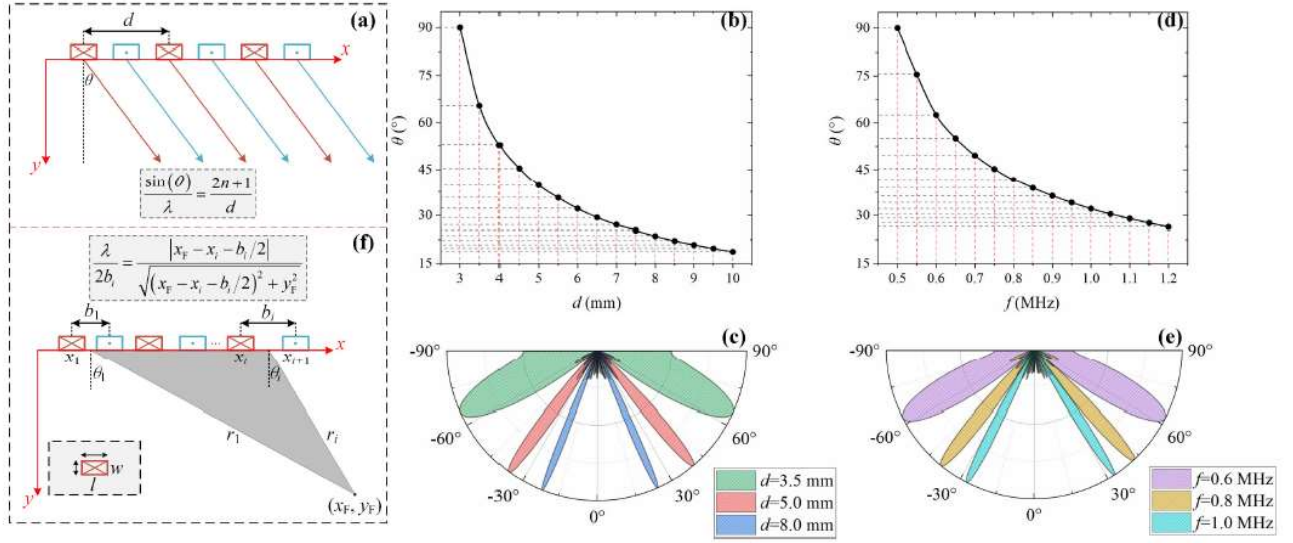


Fig. 1 Coil arrangement for beam focusing of an SH guided-wave EMAT: (a) Equally spaced coil arrangement for obliquely propagated SH guided-waves. (b) Relationship between source spacing d and radiation angle θ . (c) The directionality of ultrasonic guided-wave propagation under different values of d . (d) Relationship between drive frequency f and radiation angle θ . (e) The directionality of ultrasonic guided-wave propagation under different values of f .

shows the EMAT configuration and Fig. 2(b) is the enlarged front view. An aluminum plate is used as a wave carrier to avoid interference by magnetostrictive effects. The thickness of the aluminum plate should be reasonably designed to ensure that only SH-0-mode guided-waves are generated. In addition, a racetrack coil is used to generate SH guided-waves, and a printed circuit board (PCB) is used to implement this coil structure. To excite the SH guided-wave, based on the Lorentz force theory, we use a PPM as the background magnetic field source. Each permanent magnet is separated by a nonpermeable polylactic acid (PLA) mold. Fig. 2(c) shows the magnet arrangement in detail, where θ represents the radiation angle, (x_F, y_F) is the coordinate of the focal point, and R is the radiation distance. To ensure the phase coherence at the preset focal position, the equation in Fig. 2(c) must be satisfied while considering alternating polarity of the adjacent radiation sources. Therefore, in this way, the phase focusing of ultrasonic guided waves at a certain point can be achieved. However, it should be noted that this symmetrical EMAT structure design will also show another focal point on the other side, which is not discussed in this paper because it lacks practical research significance.

The Huygens approach uses simple assumptions that can facilitate the preliminary study of the wavefield, even if it cannot accurately describe the actual ultrasound field. When a Gaussian impulse is applied as the input signal, the wavefield can be described by the following equation:

$$\psi(t, x, y) = \sum_n (-1)^n r_n^{-0.5} e^{-\frac{(k_0 r_n - \omega_0 (t - t_0))^2}{2\omega_0^2 \delta^2}}, \quad (2)$$

where ψ is the wavefield displacement, t is the time, n is the source number, m is the distance between source n and position (x, y) , $k_0 = \omega_0 / c_s$ is the wavenumber, and δ is a constant related to the signal temporal width. The value of each factor is selected as follows: $n=6$, $f=1$ MHz, and $\delta=1$ μ s. Although it is difficult to reflect the focusing performance of this approximate calculation, the characteristics of an EMAT can be analyzed qualitatively. Fig. 2(d) shows the wavefield distribution at 40.44 μ s, and Fig. 2(e) describes two important factors affecting the wavefield intensity: angle θ from the y -axis and radiation distance r . It can be seen in Fig. 2(e) that when $\theta > 5^\circ$, the wave displacement increases nonlinearly as θ increases. However, when $\theta < 5^\circ$, the phenomenon is reversed. In addition, as θ increases, the rate of increase of the wave displacement gradually decreases. For radiation distance r , its increase will lead to a decrease in wave displacement. In other words, the intensity of the wave decays exponentially as the transmission distance increases, as shown by the blue line in Fig. 2(e).

Therefore, the focal point should not be too far from the transducer, and angle θ from the y -axis should be greater than 20° to ensure a high signal intensity. These conclusions can initially guide the design and configuration of the transducer, but more accurate results can be obtained through finite element modeling.

C. Numerical Modelling

In the simulation, we used COMSOL software to calculate the propagation of guided-waves in an aluminum plate. Electromagnetic and elastic dynamic fields are used to describe the working process of an EMAT. The design parameters are shown in Table 1.

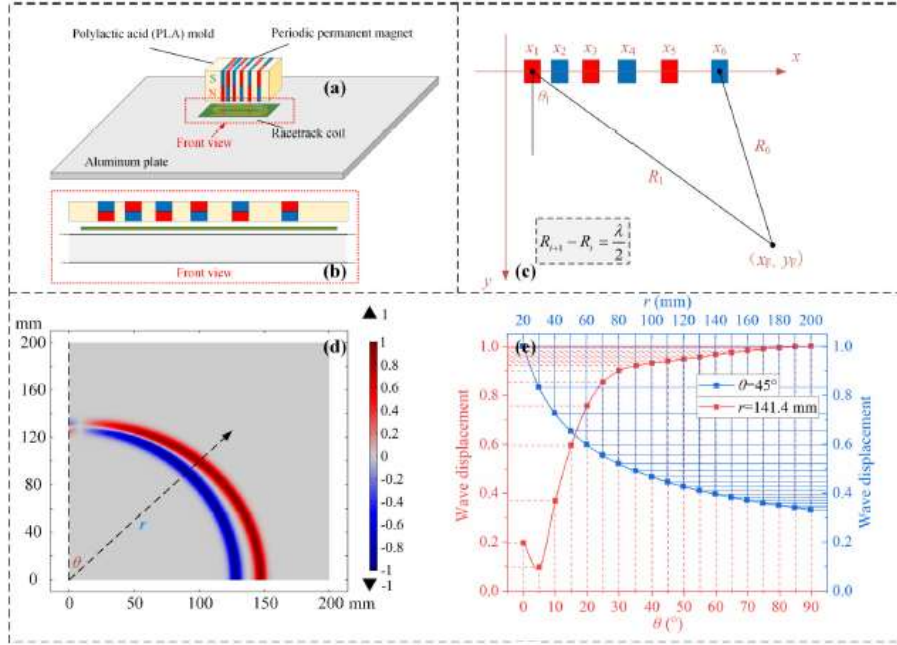


Fig. 2 Configuration and wavefield calculation of a newly designed point-focusing EMAT: (a) EMAT arrangement with the PLA mold, PPM, racetrack coil, and aluminum plate. (b) The enlarged front view of (a). (c) PPM arrangement for wave focusing. (d) Wavefield calculation at $40.44 \mu\text{s}$; θ is the angle from the y -axis, and r is the radiation distance. (e) Two important factors affecting the wavefield intensity, i.e., θ and r . When studying r , θ is fixed at 45° ; when studying θ , r is fixed at 141.4 m .

TABLE I: SIMULATION PARAMETERS

Parameter	Value
Focal position (mm)	(50,50)
Wave speed (m/s)	3200
Frequency (kHz)	500
Lift-off distance (mm)	1
Lame's constants λ (Gpa)	58
Lame's constants μ (Gpa)	29
Aluminum specimen mass density (kg/m^2)	2832
Aluminum specimen conductivity (S/m)	3.65×10^7

The x -coordinate of each unit source is calculated using the equation in Fig. 2(c): $x_1=0 \text{ mm}$, $x_2=4.64 \text{ mm}$, $x_3=9.55 \text{ mm}$, $x_4=14.86 \text{ mm}$, $x_5=20.78 \text{ mm}$, $x_6=27.79 \text{ mm}$. Fig. 3(a) shows the simulation results at the moment when the guided wave reaches the preset focal point at $24.35 \mu\text{s}$. As mentioned before, this symmetrical structure of the transducer will exhibit two symmetrical focal points. Fig. 3(b) is an enlarged view of the red dotted frame in Fig. 3(a); it can be seen that the ultrasound reaches its maximum intensity at the focal point. Fig. 3(c) shows the relationship between the displacement amplitude and time at the focal point. Since the longitudinal wave is twice as fast as the shear wave, it will appear before the S-wave, but its amplitude will be smaller. Fig. 3(d) shows a comparison of the signal intensity between the focused side and the unfocused side on the semicircle in Fig. 3(b). The center point of the coil (13.9

mm, 0 mm) is set as the circle center, and the distance between this point and the focal point is defined as the radius. Fig. 3(d) shows that the magnitude of the displacement on the focused side is nearly double that on the nonfocused side. Therefore, the newly designed point-focusing EMAT can successfully converge SH guided waves to a point.

In defect detection, the size of the focal area is an important factor affecting detection accuracy. In Fig. 3(b), the focal area is defined as a contour line that is half the displacement peak value, which is shown as a white ellipse in the figure. The vertical axis of the ellipse indicates the length L of the ultrasonic wave, and the horizontal axis indicates the wave width W . The time corresponding to the half-peak is $7.4 \mu\text{s}$ in Fig. 3 (c), and the angle corresponding to the half-peak is 18° in Fig. 3 (d). Therefore, the size of the focal area can be described as $L=23.7 \text{ mm}$ and $W=18.5 \text{ mm}$. In addition, when the focal position is (100 mm, 100 mm), the calculation result is $L=23.7 \text{ mm}$ and $W=19.3 \text{ mm}$. This is because L is related only to the width of the excitation signal, and W is related to the wave propagation distance.

III. THEORETICAL ANALYSIS

The focusing performance of an EMAT is related to many factors, including the excited current, coil structure, PPM arrangement, and specimen properties. In the design of the focusing transducer, the focal position is determined by the signal frequency and the unit source arrangement. In addition, the material properties of the test specimen are generally

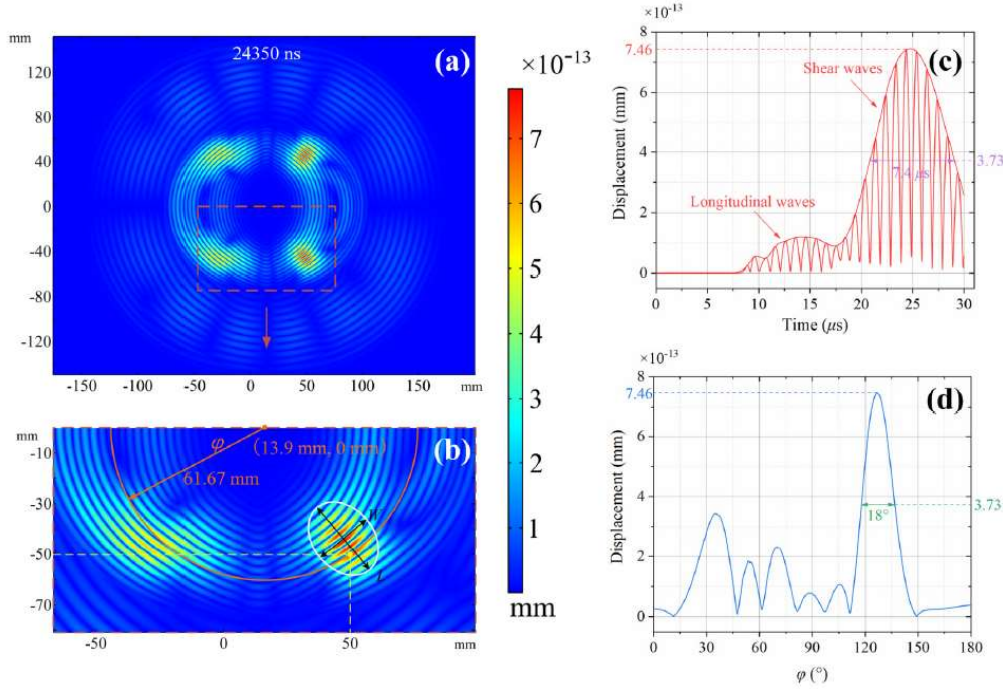


Fig. 3 Simulation results for a point-focusing SH guided-wave EMAT: (a) Simulation results of the displacement field distribution at 24.35 μs , which is the moment when the guided-wave reaches the focal point. (b) An enlarged view of the red dotted frame in (a). The center of the red semicircle is the coil center, and its radius is the distance from this center to the focal point. The white ellipse is defined as the focal area. (c) The relationship between displacement amplitude and time at the focal point. (d) The signal intensity between the focused side and the unfocused side on the semicircle in (b).

determined, but the size and number of unit sources can be changed. Therefore, it is important to study these factors to optimize the focusing capability of the transducer. Fig. 4(a) shows the definition of the unit source: l is the length of the permanent magnet, and w is twice the width of the permanent magnet. The center frequency of the excitation burst current is 1 MHz, the preset focal position is (50 mm, 50 mm), and the last unit source position is fixed at (40.456 mm, 0 mm). In the study, the central position of the unit source remains unchanged, while only its length l , width w , and source number n change. Since the change in the displacement at the focal point is an important manifestation of the focusing transducer's performance, the relationship between the displacement of the focal position with time is mainly studied, and the influence of longitudinal waves is also considered.

Figs. 4(b, c) show the influence of the change in unit source width w on the displacement at the focal point, and it can be seen from Fig. 4(b) that the unit source length l remains unchanged at 2 mm. In addition, the unit source number n is fixed at 6. Fig. 4(c) shows that as w increases, the signal amplitude of shear waves first increases and then decreases and reaches a maximum value when $w=l=2$ mm. In addition, the amplitude of the longitudinal wave increases with w , as shown in Fig. 4(c). It can be seen that with increasing w , the displacement amplitudes of the shear and longitudinal waves tend to be consistent. For unit source length l , Figs. 4(d, e) show its effect when w is fixed at 2 mm, and Fig. 4(e) shows that the displacements of the shear and longitudinal waves at the focal

point increase with the increase in l . Fig. 4(f) depicts the arrangement for all sources, and the size of n is changed, while the last unit source's coordinate remains unchanged. Therefore, Fig. 4(g) shows that as the number of unit sources n increases, the magnitude of the displacement at the focal point gradually increases.

To summarize, to obtain the best focusing performance of the newly designed EMAT, the width w of the unit source should be consistent with its length l , and its length l should be made larger within a certain range. In addition, the increase in the unit source number n is also beneficial to improving the focusing capability of the transducer.

IV. EXPERIMENT AND MEASUREMENT

To verify the focusing performance of the SH guided-wave point-focusing transducer and its capability to detect defects, we inspect different defect shapes on the aluminum plate surface. The RPR-4000 Pulsar and Receiver is used as the signal-transmitting power source and receiving device, supplemented by a necessary signal amplifier. The received signal waveform can be displayed on an oscilloscope, and a PC can process the received data. In the experiment, to avoid the signal interference caused by the boundary reflection wave, and considering the generation of the SH-0 pure guided-wave mode at 500 kHz [16], the size of the aluminum plate is $500 \times 500 \times 3$ mm³. The transmitter is the newly designed point-focusing SH

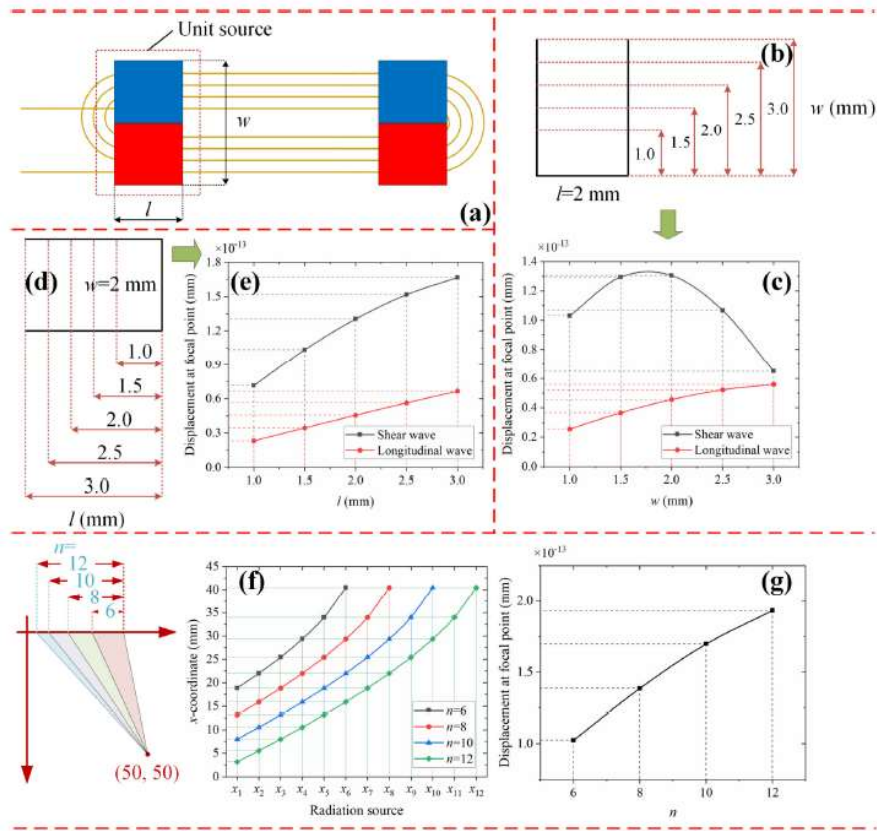


Fig. 4 Effect of the unit source arrangement on the EMAT focusing performance: (a) Transducer configuration and the definition of a unit source. (b) The sitting of the unit source size when changing w . (c) The relationship between w and the displacement at the focal point. (d) The setting of the unit source size when changing l . (e) The relationship between l and the displacement at the focal point. (f) x-coordinates for all unit sources when n changes. (g) The relationship between n and the displacement at the focal point.

guided-wave EMAT with a focal point coordinate of (100 mm, 100 mm). Two receivers are nonfocusing transducers, named Receiver X and Receiver Y, which are placed on the x-axis and y-axis, respectively.

Fig. 5(a) shows the experimental configuration in detail. There are two different defects on the aluminum specimen: the size of one is $20 \times 20 \times 1.5$ mm³, and the size of the other is $20 \times 5 \times 1.5$ mm³. The experimental results in this paper are based on square defects, while the experimental results of rectangular defects are omitted due to the similarity of methods. The racetrack coil is implemented on a PCB, with an effective length of 30 mm and a width of 4 mm. Because the PPM structures of the transmitting transducer and the receiving transducer are different, two PLA molds are fabricated using 3D printing technology: one with variable spacings and the other with an equal spacing (half wavelength). Fig. 5(b) shows a detailed method for detecting defects. The left edge coordinate x_T of the transmitter is defined as the position of the transmitting transducer. When $x_T = 0$ mm, the coordinate of the focal point is (100 mm, 100 mm), and the distance between adjacent unit sources at a 500 kHz excitation frequency is shown in Fig. 5(b). x_T varies from -30 mm to 40 mm, with steps of 2.5 and 5 mm, thereby changing the focal position to scan for defects. The

defect is located at the focal point, and the coordinates x_R and y_R are defined as their centers. Whenever the transmitting transducer moves to a new position, the receiver X scans (170-230 mm, 0 mm) in steps of 3 mm, and the receiver Y scans (0 mm, 170-230 mm) in steps of 3 mm. In this way, whether the defect exists can be determined, and its size and position information can be further obtained through calculation.

Empirical mode decomposition (EMD) method is used to determine the guided wave mode, and the time-frequency energy density precipitation method is applied for TOF extraction, which were developed in our previous studies [26, 27]. Through measurement, we can obtain the size of the received signal when x_T and x_R changes within a certain range, as shown in Fig. 6(a). Fig. 6(a) shows that the change in x_T will have a significant effect on the received signal. Due to the reflection of the defect on the guided wave, some x_T and x_R will show higher signal amplitudes. Therefore, the size of the defect in the x-direction can be obtained. For comparison purposes, the received signal amplitude is normalized to its maximum value. To further determine the defect position, the travel time of SH guided waves needs to be measured. The moments corresponding to all data points in Fig. 6(a) are shown. It can be

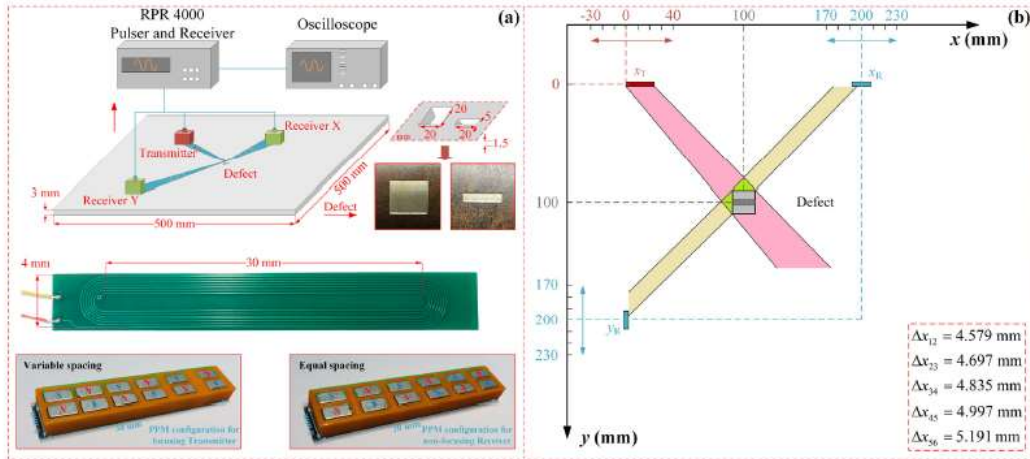


Fig. 5 Experimental configuration for detecting defects using the newly designed focusing EMAT. (a) Measurement methods, defects, coils, and PPM design. (b) The relative positional relationship and range of the transmitting transducer, the receiving transducer, and the defect.

found that the time range corresponding to most data points is 75-95 μs , and other points indicate that the receiving transducer does not receive the defect reflected wave; thus, only the direct wave along the x-axis of the transmitter is recorded. Figs. 6(b, d) show the experimental results for receiver Y; thus, the size of the defect in the y-direction can be obtained, and the precise defect location can be determined.

Fig. 6(e) shows the maximum signal obtained by the receiving transducer and its corresponding moment for different x_T values. From the corresponding time, the range of the effective defect-reflected wave signal can be obtained, and the range boundary is represented by a solid pink line. Therefore, only the effective maximum amplitude between the two pink solid lines needs to be considered. Within this range, it is assumed that the maximum amplitude is A_{max} and the minimum amplitude is A_{min} . Because the signal obtained by the receiving transducer is the total contribution value within the range of the transducer length (20 mm), to improve the measurement accuracy, the critical amplitude is defined as $A_{\text{min}} + 40\%(A_{\text{max}} - A_{\text{min}})$. Therefore, for X receivers, the critical range of x_T is 33.1 mm; for Y, it is 34.3 mm. Due to the existence of the beam width, there will be a large deviation in the measurement results. The width of the focal area is 19.3 mm through the simulation calculations mentioned above, and its x and y components are both 13.645 mm. Finally, the size of the defect can be obtained: 19.5×20.7 mm², as shown in Fig. 6(f); the results for the rectangular defect are also shown. In addition, in the calculation of the defect position, since each point within the effective x_T range contributes, its coordinates can be calculated by the following equation:

$$x_{\text{defect}} = \frac{1}{N} \sum_{i=1}^N \left(x_{T_i} + \frac{t_i c_s}{2\sqrt{2}} \right), \quad (3)$$

$$y_{\text{defect}} = \frac{1}{N} \sum_{i=1}^N \frac{t_i c_s}{2\sqrt{2}}, \quad (4)$$

Fig. 6(f) shows the results for the square and rectangular defects. The right and bottom edges of the defect are speculable because the shape of the defect is known. If the shape of the defect is unknown, the same scan needs to be performed again on the opposite side, and the position of the transducer is required to be changed accordingly. It can be found that the error between the measurement result and the actual defect is small, which proves the effectiveness of the newly designed focusing EMAT.

V. CONCLUSIONS

In this work, by changing the structure of the PPM, directional beam focusing and phase-coherence point focusing of SH guided waves can be achieved. Since the latter offers effective solutions to the low energy conversion efficiency of EMATs, we conducted further research on the newly designed phase-focusing EMAT. By approximate wave field calculation of the analytical equations, the following conclusions were obtained: as the source spacing d increases, the radiation angle θ and beam width decrease. From the wavefield calculation, it can be determined that the closer to the axis of the transducer and to the transducer itself, the higher the signal intensity. In a more accurate finite element simulation, it can be seen that the signal intensity at the focal point position is nearly double that of the nonfocusing side. To obtain the best focusing performance of the newly designed EMAT, the size and number of unit radiation sources are studied in the simulation. With this purpose, the width w of the unit source should be consistent with its length l , and its length l should be set to a larger value within a certain range. In addition, increasing the unit source number n is also beneficial as it improves the focusing capability of the transducer. It is found in the experiments that this new focusing transducer can more accurately determine the size and location of defects, thereby proving the effectiveness of the proposed point-focusing SH guided-wave EMAT in defect detection.

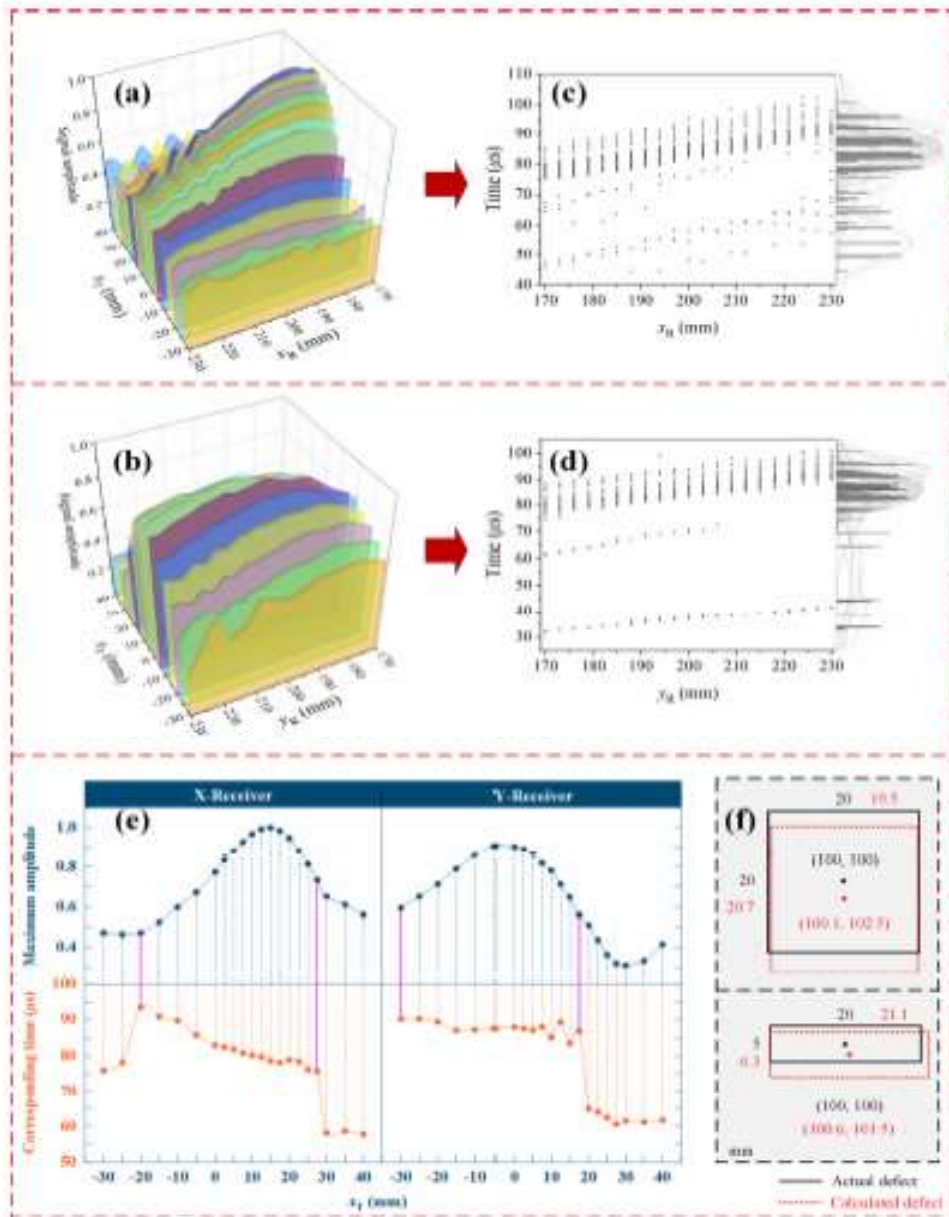


Fig. 6 Experimental results. (a, b) Received signal amplitude for different x_T values of receivers X and Y; different colors indicate different x_T values. (c, d) Received signal moment for different x_T values of receivers X and Y. The histogram and curve on the right-hand side indicate the occurrence frequency of time data. (e) Maximum signal amplitudes and corresponding times for different x_T values. The solid pink line indicates the boundary of the critical x_T . (f) The size and location of the defects obtained from the experiment, as well as the actual size and location of the defects (the right and lower edges of the defect are speculative because the defect shape is known).

ACKNOWLEDGMENT

This research was supported by the National Key R&D Program of China (Grant No. 2018YFF01012802), National Natural Science Foundation of China (NSFC) (No. 51677093) and National Natural Science Foundation of China (NSFC) (No. 51777100).

REFERENCES

- [1] Legendre, S. et al. Neural classification of Lamb wave ultrasonic weld testing signals using wavelet coefficients. *IEEE Trans. Instrum. Meas.* **50**, 672-678 (2001).
- [2] Huang, S. et al. An Opening Profile Recognition Method for Magnetic Flux Leakage Signals of Defect. *IEEE Trans. Instrum. Meas.* **68**, 2229- 2236 (2019).
- [3] Seung, H., Park, C., Kim, Y. An omnidirectional shear-horizontal guided wave EMAT for a metallic plate.

- Ultrasonics. 69, 58-66 (2016) *Mechanics*, vol. 52, no. 3-4, pp. 991-998, 2016.
- [4] Hirao, M., Ogi, H. An SH-wave EMAT technique for gas pipeline inspection. *NDT&E Int.* 32, 127-132 (1999).
- [5] Li, J., Rose, J. Natural beam focusing of non-axisymmetric guided waves in large-diameter pipes. *Ultrasonics*. 44, 35-45 (2006).
- [6] Kang, L. et al. Enhancement of ultrasonic signal using a new design of Rayleigh-wave electromagnetic acoustic transducer. *NDT&E Int.* 86, 36- 43 (2017).
- [7] Augustyniak, M., Usarek, Z. Finite Element Method Applied in Electromagnetic NDTE: A Review. *J. Nondestruct. Eval.* 35, (2016)
- [8] Dhayalan, R., Balasubramaniam, K. A hybrid finite element model for simulation of electromagnetic acoustic transducer (EMAT) based plate waves. *NDT&E Int.* 43, 519-526 (2010).
- [9] Mirkhani, K. et al. Optimal design of EMAT transmitters. *NDT&E Int.* 37, 181-193 (2004).
- [10] Ludwig, R. Theoretical basis for a unified conservation law description of the electromagnetic acoustic transduction process. *IEEE Trans. Ultrason Ferr.* 39, 476-480 (1992).
- [11] Xu, T., Zhao, L., Jiang, Z. An Analytical Equivalent Circuit Model for Optimization Design of a Broadband Piezoelectric Micromachined Ultrasonic Transducer With an Annular Diaphragm. *IEEE Trans. Ultrason Ferr.* 66, 1760-1776 (2019).
- [12] Nurmalia, Mode conversion behavior of SH guided wave in a tapered plate. *NDT&E Int.* 45, 156-161 (2012).
- [13] Sun, F., Sun, Z., Chen, Q., Murayama, R. Characteristics of SH₀-wave Converted to T(0, 1)-wave Based on a T-shaped Plate Wrapped Around a Pipe. *IEEE Trans. Ultrason Ferr.* 66, 129-137 (2019).
- [14] Clough, M., Fleming, M., Dixon, S. Circumferential guided wave EMAT system for pipeline screening using shear horizontal ultrasound. *NDT&E Int.* 86, 20-27 (2017).
- [15] Tkocz, J., Dixon, S. Electromagnetic acoustic transducer optimisation for surface wave applications. *NDT&E Int.* 107, 102142 (2019).
- [16] Sun, H. et al. Point-Focusing of Shear-Horizontal Wave Using Fan- Shaped Periodic Permanent Magnet Focusing Coils EMAT for Plate Inspection. *IEEE Sens. J.* 19, 4393-4404 (2019).
- [17] Sun, H. et al. Improvement of unidirectional focusing periodic permanent magnet shear-horizontal wave electromagnetic acoustic transducer by oblique bias magnetic field. *Sensors and Actuators: A. Physical.* 290, 36- 47 (2019).
- [18] Song, X., Qiu, G. Optimization of a focusable and rotatable shear-wave periodic permanent magnet electromagnetic acoustic transducers for plates inspection. *Sensors*. 17, 2722 (2017).
- [19] Thring, C., Fan, Y., Edwards, R. Focused Rayleigh wave EMAT for characterisation of surface-breaking defects. *NDT&E Int.* 81, 20-27 (2016).
- [20] Ogi, H., Hirao, M., Ohtani, T. Line-focusing of ultrasonic SV wave by electromagnetic acoustic transducer. *J. Acoust. Soc. Am.* 103, 2411-2415 (1998).
- [21] Ogi, H., Hirao, M., Ohtani, T. Line-focusing electromagnetic acoustic transducers for the detection of slit defects. *IEEE Trans. Ultrason Ferr.* 46, 341-346 (1999).
- [22] G. Alers, D. MacLauchlan, "High frequency, angle beam EMATs for weld inspection," in *Review of Progress in Quantitative Nondestructive Evaluation*, ed. D. O. Thompson and D. E. Chimenti (Plenum, New York) vol. 2A, p. 271, 1982.
- [23] Hill, S., Dixon, S. Frequency dependent directivity of periodic permanent magnet electromagnetic acoustic transducers. *NDT&E Int.* 62, 137-143 (2014).
- [24] Dixon, S., Hill, S., Fan, Y., Rowlands, G. The wave-field from an array of periodic emitters driven simultaneously by a broadband pulse. *J. Acoust. Soc. Am.* 133, 3692-3699 (2013).
- [25] S. Huang, et al., Unidirectional Focusing of Horizontally Polarized Shear Elastic Waves Electromagnetic Acoustic Transducers for Plate Inspection. *J. Appl. Phys.* 125, 164504 (2019).
- [26] Y. Zhang, S. Huang, S. Wang, W. Zhao. "Time-Frequency Energy Density Precipitation Method for Time-Of-Flight Extraction of Narrowband Lamb Wave Detection Signals," *Review of Scientific Instruments*, vol. 87, no. 5, pp. 054702, 1-8, 2016.
- [27] Y. Zhang, et al., "Recognition of Overlapped Lamb Wave Detecting Signals in Aluminum Plate by EMD-Based STFT Flight Time Extraction Method," *International Journal of Applied Electromagnetics and Mechanics*, vol. 52, no. 3-4, pp. 991-998, 2016.